Applied Catalysis B: Environmental 94 (2010) 241–247

Contents lists available at ScienceDirect

Applied Catalysis B: Environmental

journal homepage: www.elsevier.com/locate/apcatb

Facile preparation of high performance visible light sensitive photo-catalysts

Hyeong Jin Yun [a], Hyunjoo Lee [b,*], Ji Bong Joo [a], Nam Dong Kim [a], Mi Yeong Kang [a], Jongheop Yi [a,*]

[a] School of Chemical and Biological Engineering, Institute of Chemical Processes, Seoul National University, Seoul 151-742, Republic of Korea
[b] Department of Chemical and Biomolecular Engineering, Yonsei University, Seoul 120-749, Republic of Korea

ARTICLE INFO

Article history:
Received 22 September 2009
Received in revised form 15 November 2009
Accepted 21 November 2009
Available online 27 November 2009

Keywords:
Carbon doping
TiO_2
Nanoparticle
Visible light
Photo-catalyst

ABSTRACT

Since the conversion of solar energy to electric or chemical forms is essential for achieving a sustainable society, the development of novel photo-catalytic materials is a subject of considerable interest. Here we report on the facile synthesis of a visible light sensitive photo-catalyst by doping a large amount of carbon into TiO_2 nanoparticles. The findings show that carbon is clearly incorporated into the TiO_2 framework, as evidenced by TPO, XANES, and EXAFS. The photo-catalytic activity of the carbon-doped TiO_2 is increased by more than 4 times, compared to commercial TiO_2 P25 for the degradation of phenol under irradiation by white light. Additionally, we observed for the first time that the carbon-doped TiO_2 shows catalytic activity under irradiation by visible light at wavelengths longer than 600 nm. The synthetic method developed in this study is very simple, and doping level of carbon can be easily controlled by changing the synthetic conditions used.

1. Introduction

TiO_2 has attracted considerable interest as a photo-catalyst for various applications [1–11], but it has a critical limitation in that electrons and holes (e^-/h^+) can be generated under conditions of UV irradiation due to its wide band-gap energy (E_g; 3.2 eV). Impurity doping has been regarded as a promising strategy for the synthesis of visible light sensitive photo-catalysts [12–25]. Among such techniques, carbon-doped TiO_2 (C–TiO_2) represents such an attractive materials, because of its superior photo-catalytic performance under visible light irradiation [12,19–25]. Because carbon doping can provide more excess electrons in the design of strong n-type semiconductors, it can induce a substantial decrease in E_g [13,24]. Moreover, elemental carbon on a TiO_2 surface can play a significant role as a photo-sensitizer in photo-catalytic reactions [25,26].

Since Khan et al. first introduced doping of carbon into TiO_2 sheet [19], attempts have been made to insert carbon into a TiO_2 framework. The first study described the use of the flame pyrolysis of a titanium sheet [19], but the resulting material comprised of film-type rutile phases which show worse photo-catalytic performance than pure TiO_2 anatase. Oxidative annealing of TiC was introduced for a simple preparation of C–TiO_2 [20], but it is difficult to incorporate a high amount of carbon into the TiO_2 framework and achieve a uniform doping level. Chemical vapor deposition (CVD) was also attempted, but it requires expensive equipment and the process is complicated [21]. Using a grinding technique also entails difficulties in doping a higher amount of carbon into TiO_2 [23].

In this work we introduce a facile synthesis of C–TiO_2 nanoparticle by wet chemistry. Capping agents are widely used for synthesis of novel nanomaterials with a uniform size and shape. We found that oleic acid, negatively charged capping agent, can be applied to incorporate carbons into TiO_2 framework. Carbon doping was accomplished via adsorption of carboxyl group from oleic acid on TiO_2 seed materials. It opens a facile route which enables to dope impurity during the synthetic process of TiO_2 nanoparticles. This method allows for doping a high amount of carbon which makes it possible to activate C–TiO_2 with a high efficiency under visible light irradiation. It should also be noted that the doping level can be easily controlled by changing the synthesis conditions appropriately. In addition to doping of carbon into TiO_2 framework, the adsorbed carbon on the TiO_2 surface can act as photo-sensitizer improving catalytic activity much further by enhancing photo-excitation. Thus photo-catalytic activity on C–TiO_2 nanoparticles can be enhanced significantly under irradiation with a long wavelength light. Nanoparticulated C–TiO_2 can also present a high charge transfer rate because of their enormous surface area. The combination of carbon doping, photo-sensitizing carbons, and a high surface area bestows outstanding photo-catalytic activities on C–TiO_2 nanoparticles under visible light irradiation.

* Corresponding authors.
E-mail addresses: azhyun@yonsei.ac.kr (H. Lee), jyi@snu.ac.kr (J. Yi).

0926-3373/$ – see front matter © 2009 Elsevier B.V. All rights reserved.
doi:10.1016/j.apcatb.2009.11.014

2. Experimental

2.1. Synthesis of carbon-doped TiO_2 nanoparticles

C–TiO_2 nanoparticles were synthesized by a gel–sol method. The gel–sol method was originally introduced by Sugimoto et al. [27,28] to synthesize TiO_2 nanoparticles from a gel-type of titanium precursor through transformation to a sol. We modified this method for the large scale synthesis of C–TiO_2 nanoparticles. A total of 0.2 mol of titanium tetraisopropoxide (TTIP, Advanced Materials Institute Co., Ltd., 98%) was added to 0.4 mol of triethanolamine (TEOA, Sigma, 98%, a gelation agent); deionized water (DI water) was then added to give 400 ml of an aqueous solution. Thirty milliliters of this solution was mixed with 30 ml of an aqueous solution of 0.02 M of oleic acid (OA, Samchun, 99.9%). This mixture was placed in a Teflon-lined autoclave and heated at 100 °C for 12 h to form a $Ti(OH)_4$ gel, then heated at 250 °C for 48 h, yielding a brown C–TiO_2 precipitate. The precipitate was centrifuged at 3000 rpm for 10 min and washed several times with DI water to remove residual surfactants. Finally, C–TiO_2 powder was obtained by drying at 70 °C for 12 h.

The amount of carbon dopant was adjusted by changing pH of the reactant solution. The initial pH of the reaction medium was varied from 7 to 11 by adding 1 M of nitric acid or sodium hydroxide with rigorous stirring at room temperature before gelation step. The pH cannot be controlled to lower than 7 due to degradation of the gel solution.

2.2. Characterizations of C–TiO_2 nanoparticles

The shapes of the synthesized C–TiO_2 nanoparticles were characterized using an energy-filtering transmission electron microscope (EF-TEM, Libra 120-Carl Zeiss, 80 kV). The microstructure was examined using a high-resolution transmission electron microscope (HR-TEM, JEM 3010-JEOL, 300 kV), X-ray diffractometer (XRD, D/max-2500/PC-Rigaku) with CuKα radiation (wavelength = 0.154 nm) as an incident beam worked at 50 kV and 100 mA. X-ray absorption near edge structure (XANES) and extended X-ray absorbance fine structure (EXAFS) analyses were performed, to investigate the atomic configurations in the C–TiO_2 nanoparticles. They were recorded at the 3C1 beamline at the Pohang Accelerator Laboratory. The X-ray absorption of titanium atoms was measured in the transmission mode around the Ti K-edge (4966 eV) by detuning in the range of 70% to eliminate higher harmonics.

Temperature programmed oxidation (TPO) measurements were made at temperatures up to 700 °C at a rate of 5 °C/min under a O_2/He gas flow. The ratio of O_2 and He was 1:9 and the flow rate of the gas mixture was 20 ml/min. A gas chromatograph (M600D-Young Lin) equipped with a thermal conductivity detector was used to analyze the outlet gas.

Optical absorbance spectra were examined by ultraviolet diffuse reflectance spectroscopy (UV-DRS, V670-Jasco) and Fourier transform-infrared spectroscopy (FT-IR, M-Seires-MIDAC).

2.3. Characterizations of photo-catalytic activities

Electrochemical analyses were performed using a standard three-electrode cell with a platinum-coated titanium mesh of 2.5 cm^2 used as the counter electrode. The substrate was ITO glass (1.5 cm × 1.5 cm), and a total of 0.4 mg of samples was deposited on the ITO glass, which served as a working electrode for chronoamperometry experiments. The total weight of deposited sample was measured on a micro-balance (CPA250D-Satorius). A saturated Ag/AgCl electrode was used as the reference electrode. The test electrolyte was prepared by dissolving $NaClO_4$ (Samchun, 98%) at a concentration of 0.1 M in deionized water. Chronoamperometry experiments were conducted using a computer-controlled potentiostat (Iviumstat, Ivium).

For investigations of photo-catalytic performance, a total of 0.15 g of each powder was suspended in 100 ml of an aqueous phenol solution under vigorous stirring. A Xe arc lamp (200 W, Oriel) was used as the light source for visible light irradiation for the photo-catalytic reactions. Optical filters were used to eliminate UV radiation during visible light experiments. All optical filters were supplied by Edmund Optics. A colored glass filter (>420, 500, 600 nm) was used to irradiate various wavelengths of visible light during the photo-catalysis experiments. In order to estimate band-gap energy by measuring the photo-generated current density under specific wavelength light illumination, a band pass glass filter (450, 500, 550, 650, 700 nm) was used during the chronoamperometry experiments.

The concentrations of phenol were measured by high performance liquid chromatography (HPLC, YL9100-Young Lin Instrument). Target compounds were quantified using HPLC on a 150 mm × 4.6 mm Zorbax Eclipse XDB-C18 column connected to a UV detector (YL9120-Young Lin Instrument). The detection wavelength was set at 210 nm. The mobile phase was a 40% aqueous solution of acetonitrile, pumped at a flow rate of 1 ml/min. A total of 20 μl of sample was injected into the column. Before injection into the column, photo-catalysts were separated from the phenol solution by filtration, followed by guard column in order to prevent additional inflow of remained photo-catalyst into HPLC column.

3. Results and discussion

3.1. Characterization of carbon-doped TiO_2 nanoparticle

C–TiO_2 nanoparticle was obtained via a dissolution–recrystallization process from highly viscous $Ti(OH)_4$ gel with the presence of oleic acid in homogeneous nucleation systems. Negatively charged carboxyl group from oleic acid was well adsorbed on the surface of TiO_2 seed materials then provided carbon dopant into TiO_2. As-synthesized C–TiO_2 powders are brown in color, indicating a heavy absorbance of light in a wide wavelength range. As shown in Fig. 1, C–TiO_2 nanoparticles show a monodispersed distribution in their shape and size. Lattice arrays of synthesized nanoparticles show interplanar distances corresponding to [1 0 1] and [0 0 2] indicating an anatase structure. It is in agreement with X-ray diffraction patterns showing only the presence of anatase structure without any other crystal phase such as rutile or brookite (Fig. 2A). The characteristic peaks of C–TiO_2 nanoparticles, however, are slightly shifted to higher 2θ values compared to pure anatase-structured TiO_2 due to the distortion of TiO_2 anatase crystal lattice (Fig. 2B). The slight distortion of the TiO_2 crystalline structure comes from positioning of carbon in TiO_2 framework because of the difference in atomic radius of oxygen and carbon. Thus the peak shift can be indirect evidence of carbon incorporation into TiO_2 crystal framework. It also should be noted that graphitic carbon peak was not observed in XRD.

In particular the amount of carbon dopant can be easily adjusted via controlling zeta potential of TiO_2 seed materials. In order to vary surface charge of the TiO_2 seed materials, we controlled the pH of the reaction medium from 7 to 11. Synthetic pH cannot be controlled lower than 7 due to degradation of the gel solution. At a lower pH of approximately 7, the negatively charged carboxyl group is more readily adsorbed to the surface of seed materials, thus enable to dope a higher amount of carbon. The amount of doped carbon was measured by elemental analysis after heat treatment at 320 °C to exclude the carbons adsorbed on the TiO_2 surface. The amount varied from 6.5 to 0.6 at.% (atomic fraction) when the pH was increased from 7 to 11. Among them,

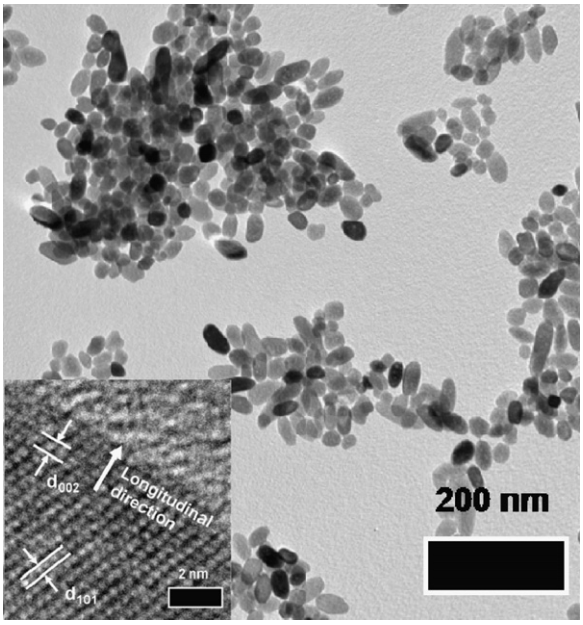

Fig. 1. TEM image of C–TiO_2 nanoparticles. C–TiO_2 nanoparticles have average dimensions of 43.0 ± 8.7 nm in length and 22.9 ± 2.8 nm in width. The inset shows the interplanar distances in the crystal lattice indicating a TiO_2 anatase structure and C–TiO_2 nanoparticles are elongated in the [0 0 1] direction of the anatase phase.

the C–TiO_2 sample synthesized at pH 9 (no nitric acid or sodium hydroxide added) was used for characterizations in this study.

3.2. Characterization of carbon dopant in C–TiO_2 nanoparticle

In order to investigate the characteristics of carbon in C–TiO_2 nanoparticles, TPO experiments were carried out in the temperature range of 100–700 °C (Fig. 3A). The consumption of oxygen began at around 200 °C, a temperature at which organic compounds that remain on a nanoparticle surface undergo combustion. And then another oxygen consumption peak was observed at around 340 °C, where elemental carbons placed on the C–TiO_2 nanoparticle surface were thermally oxidized. At 410 °C the last peak was observed, which is related to the combustion of doped carbon. Elemental analysis showed that there are 7.9 at.% of carbons in TiO_2 nanoparticles as adsorbed on the surface or doped into the crystalline framework. More than 99% of the carbons were eliminated after the TPO treatment until 700 °C. The atomic ratio of adsorbed and incorporated carbon was calculated via comparing the integration of each curve which was deconvoluted from TPO results. The amount of adsorbed carbons on the C–TiO_2 is 1.5 times more than incorporated carbons in the C–TiO_2 nanoparticles.

For further characterizations of C–TiO_2 nanoparticles, we carried out heat treatments at various temperatures, 200, 250, 320, and 450 °C under the atmospheric condition based on TPO results. (Labeled as C–TiO_2-200, 250, 320, 450, respectively.) The organic compounds with hydrocarbon chains remained on the surface of C–TiO_2-200 as checked by large sp^3 C–H stretching peaks in FT-IR (Fig. 4). After calcinations at 250 °C, organic compounds were completely eliminated from the nanoparticle surface as evidenced by the disappearance of sp^3 C–H stretching peaks. Interestingly, the color of the powder became dark brown after the heat treatment at 250 °C as shown in Fig. 3B. It was caused by a thickened carbon layer as the result of the carbonization of residual organic compounds. Since the graphitic carbon peak was not observed in XRD, the carbon seems to exist as elemental carbons on TiO_2 surface. After removing the elemental

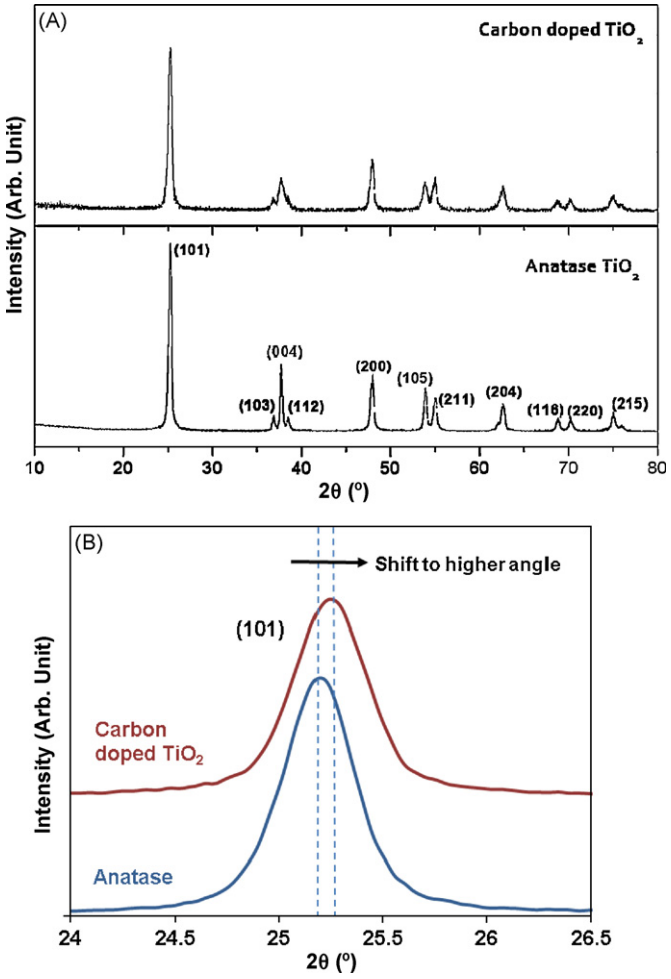

Fig. 2. (A) XRD patterns of C–TiO_2 nanoparticles indicate the presence of only an anatase structure without any other crystal phase such as rutile or brookite. (B) Shift of XRD pattern due to crystalline distortion of anatase framework caused by carbon doping.

carbons by combustion at 320 °C, the detected carbon on C–TiO_2-320 is carbon that had been incorporated into the TiO_2 framework and not located on the nanoparticle surface. The light brown colored C–TiO_2-320 contained 3.9 at.% of carbon. The doped carbon was completely removed from the TiO_2 nanoparticles after calcination at 450 °C, at which point the color of the powder was pure white.

XANES and EXAFS analyses were performed to investigate the atomic configurations in the C–TiO_2 nanoparticles. XANES spectra, taken around the Ti K-edge of C–TiO_2 nanoparticles are presented in Fig. 5A. Pre-edge region of XANES shows the information about coordination environments of Ti in C–TiO_2. The pre-edge peaks, A1, A2, and A3 arise from transitions from Ti 1s energy levels to bound Ti 3d (or O 2p) molecular orbitals. The coordination number can be provided from the relations between normalized pre-edge peak (A2) intensity and photon energy position. The normalized intensity of 0.22 at 4971 eV for the XANES spectrum indicates a sixfold coordination environment around the Ti atom in C–TiO_2, which is typical for anatase-structured TiO_2 [29,30]. The fact that the anatase structure for the C–TiO_2 nanoparticles is preserved indicates that the doped carbon is substitutionally interposed in the TiO_2 framework replacing oxygen atom. The cationic substitutional incorporation of a carbon for a Ti atom seems less likely due to the strong distortion of the framework resulting from the large difference in the bonding length of Ti–O and C–O and the electronic instability resulting from different coordination numbers [24]. As

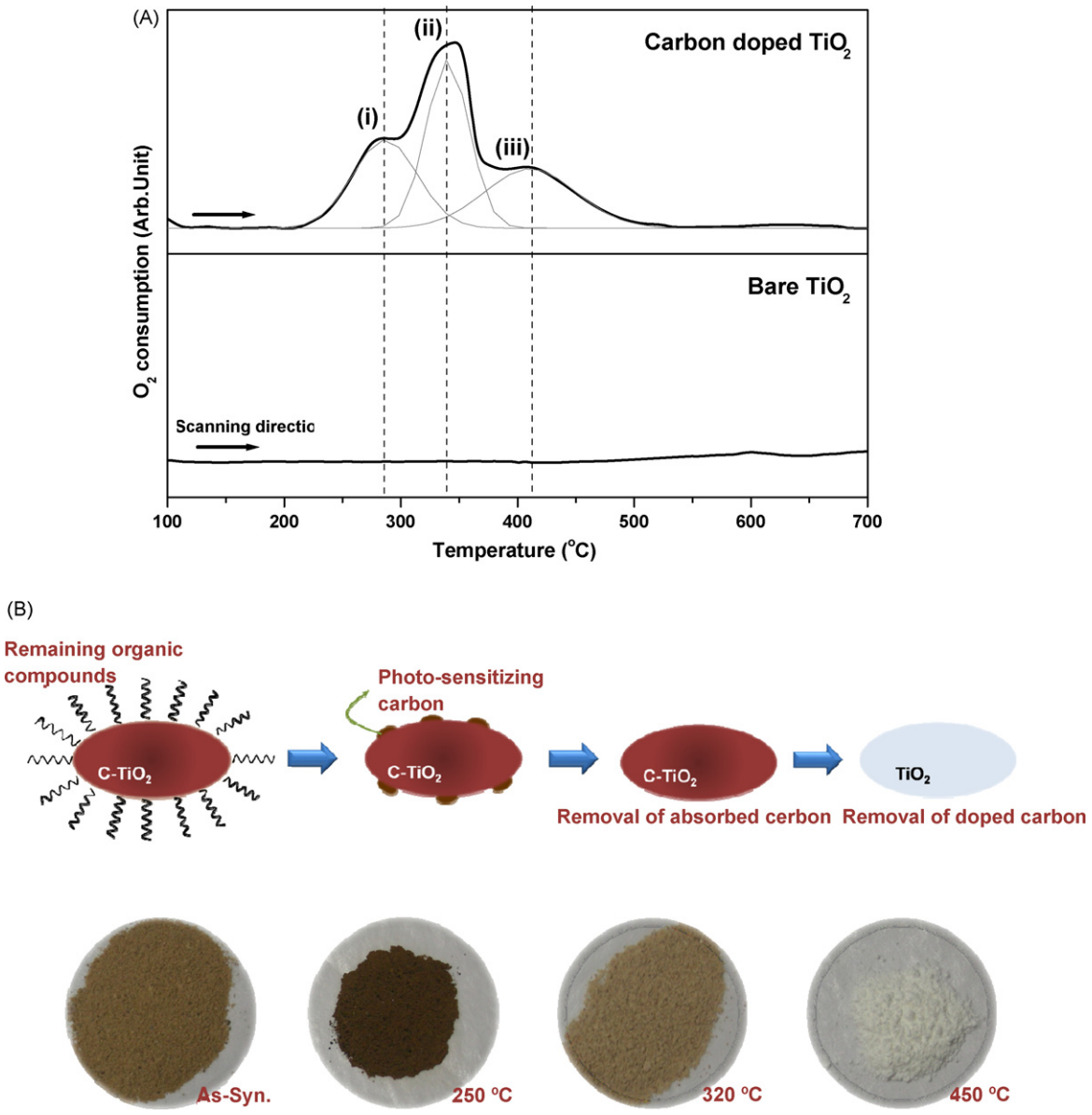

Fig. 3. (A) TPO experimental results. Three oxygen consumption peaks were observed in case of C–TiO_2 nanoparticles. (i) Combustion of residual organic compounds, (ii) thermal oxidation of photo-sensitizing carbon located on the C–TiO_2 nanoparticle surface, and (iii) thermal oxidation of doped carbon that had been incorporated into the anatase framework. No peaks were observed in case of bare TiO_2. (B) Schematic diagrams of removal sequence of carbon from C–TiO_2 nanoparticles and photographs of samples calcined at various temperatures.

shown in Fig. 5B, EXAFS spectra of the C–TiO_2 nanoparticles are similar to the typical spectrum of anatase, as previously reported [30,31], except for a slight shift to higher bond length. The interatomic distance of Ti–O and Ti–Ti in the C–TiO_2 nanoparticles becomes longer than pure anatase-structured TiO_2 due to the larger bonding length of Ti–C [24], while the sixfold coordination environment around Ti atoms remained unchanged. After the heat treatment up to 320 °C, the EXAFS spectrum pattern did not change significantly, indicating that doped carbon does not undergo any significant change at temperatures up to 320 °C while adsorbed carbon was removed. In the case of C–TiO_2-450, however, the peaks were shifted to lower bonding length corresponding to a pure anatase structure with a TiO_6 octahedral structure (1.96 and 3.04 Å for Ti–O and Ti–Ti, respectively). The carbon absorbed to the surface, was removed with increasing calcination temperature, and the carbon that had been incorporated into the TiO_2 framework then become unstable and oxidized with the crystalline structure preserved.

3.3. Measurement of band-gap energy

The band-gap energy of each sample was determined from UV-DRS spectra (Fig. 6A). The as-synthesized C–TiO_2 nanoparticles showed a E_g of about 2.3 eV, indicating that e^-/h^+ pairs can be generated when the particle is irradiated with visible light. In particular the absorbance spectrum of C–TiO_2-250 was shifted upward, compared to as-synthesized C–TiO_2, because it absorbs more photons in a broad wavelength range due to a large amount of carbon located on the nanoparticle surface. After calcinations at 450 °C, the absorbance was very similar to that of pure anatase-structured TiO_2 due to the complete elimination of doped carbon. Electrochemical technique was also used to determine E_g values. It is reported that the optical absorption near the band edge is given as follows [32]:

$$\alpha = \frac{A(h\nu - E_g)^2}{h\nu} \quad (1)$$

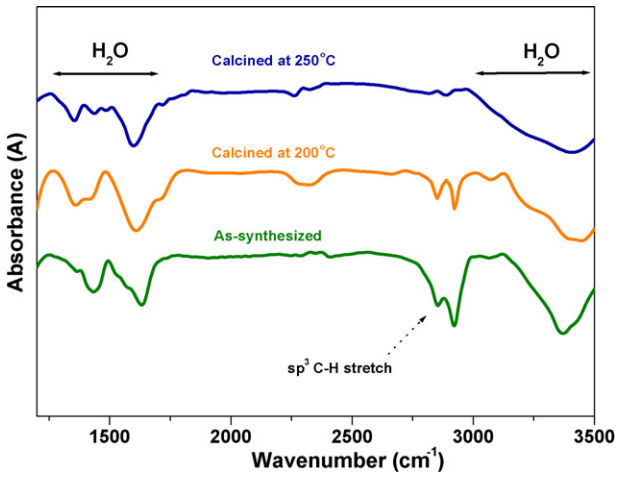

Fig. 4. FT-IR spectra of C–TiO_2 nanoparticles. Peaks corresponding to sp^3 C–H stretching disappeared with an increase in heat treatment temperature. Organic compounds with hydrocarbon chains remained on the surface of C–TiO_2-200 as evidenced by the large sp^3 C–H stretching peaks. After calcination at 250 °C, the organic compounds were eliminated from the surface of nanoparticles, as evidenced by the disappearance of sp^3 C–H stretching peaks.

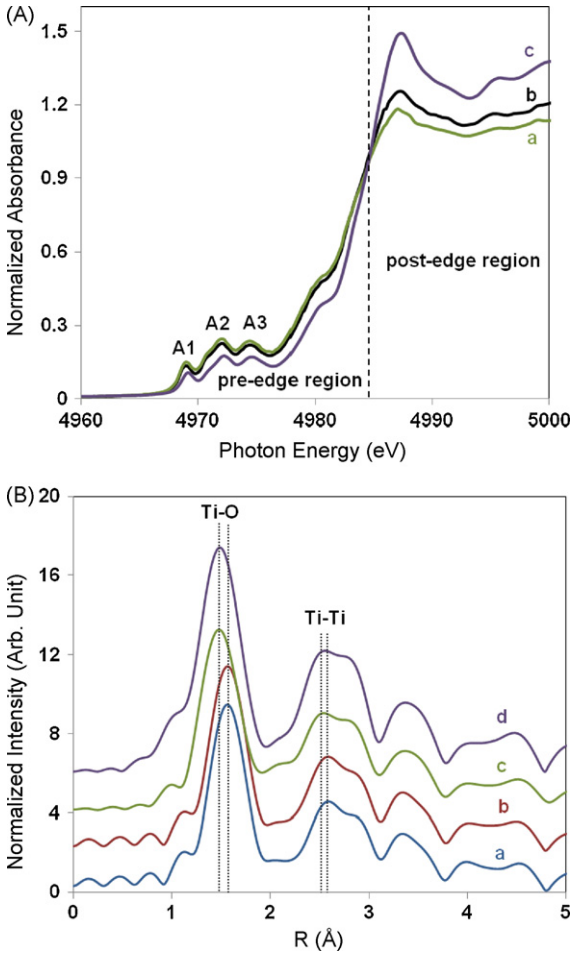

Fig. 5. (A) XANES spectra of (a) as-synthesized C–TiO_2, (b) C–TiO_2-450, and (c) anatase TiO_2. Preservation of TiO_2 anatase structure for the C–TiO_2 nanoparticles reveals that doped carbon is substitutionally interposed in TiO_2 framework. (B) EXAFS spectra of (a) as-synthesized C–TiO_2, (b) C–TiO_2-320, (c) C–TiO_2-450, and (d) anatase TiO_2. There were no observed changes in EXAFS spectra in the case of C–TiO_2-250 and C–TiO_2-320. After heat treatment at 450 °C, the interatomic distances were reduced to the value corresponding to octahedral TiO_6.

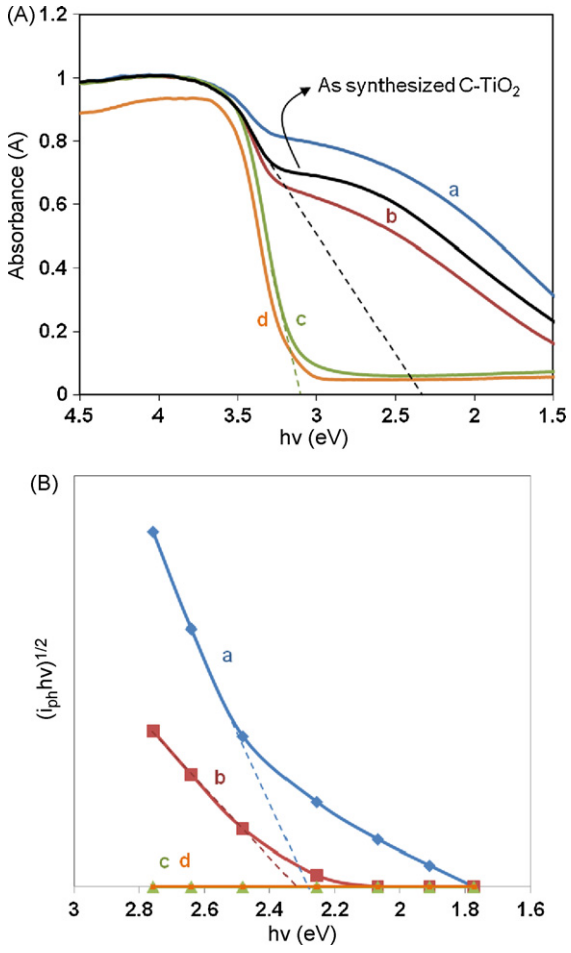

Fig. 6. (A) UV visible diffused reflectance spectrum and (B) determination of E_g values from $(i_{ph}h\nu)^{1/2}$ versus $h\nu$ plots in the range of visible light; (a) C–TiO_2-250, (b) C–TiO_2-320, (c) C–TiO_2-450, and (d) anatase TiO_2.

where α is an absorption coefficient, A, a constant, E_g, the band-gap energy. Since the photo-generated current density (i_{ph}) is proportional to α, E_g can be determined from a plot of $(i_{ph}h\nu)^{1/2}$ versus $h\nu$ [22] (Fig. 6B). The value of E_g for as-synthesized samples cannot be estimated by electrochemical methods because the measured photo-generated current density involves the oxidation current density of residual organic compounds on the surface of the nanoparticles. The E_g values for C–TiO_2-250 and C–TiO_2-320 were not significantly different (2.3 and 2.33 eV respectively) due to small amount of change in the amount of doped carbon. The band-gap energies measured by this electrochemical measurement are in reasonably good agreement with optical measurements by UV-DRS. C–TiO_2-450 and P25 can generate no current density in visible light region.

3.4. Photo-catalytic performance under visible light

To investigate photo-catalytic performances under visible light, we carried out the photo-catalytic oxidative decomposition of phenol under irradiation by white (≥420 nm), green (≥500 nm), and red (≥600 nm) light (Fig. 7). The photo-catalytic performance of C–TiO_2-250 was superior to that for the other samples including commercial TiO_2 photo-catalyst P25 under the various illumination conditions. The large difference in reactivity of C–TiO_2-250 and C–TiO_2-320 was caused by the presence of photo-sensitizing carbon on C–TiO_2 surface. It aids in producing superoxide radicals by transferring electrons to the conduction band of TiO_2 under

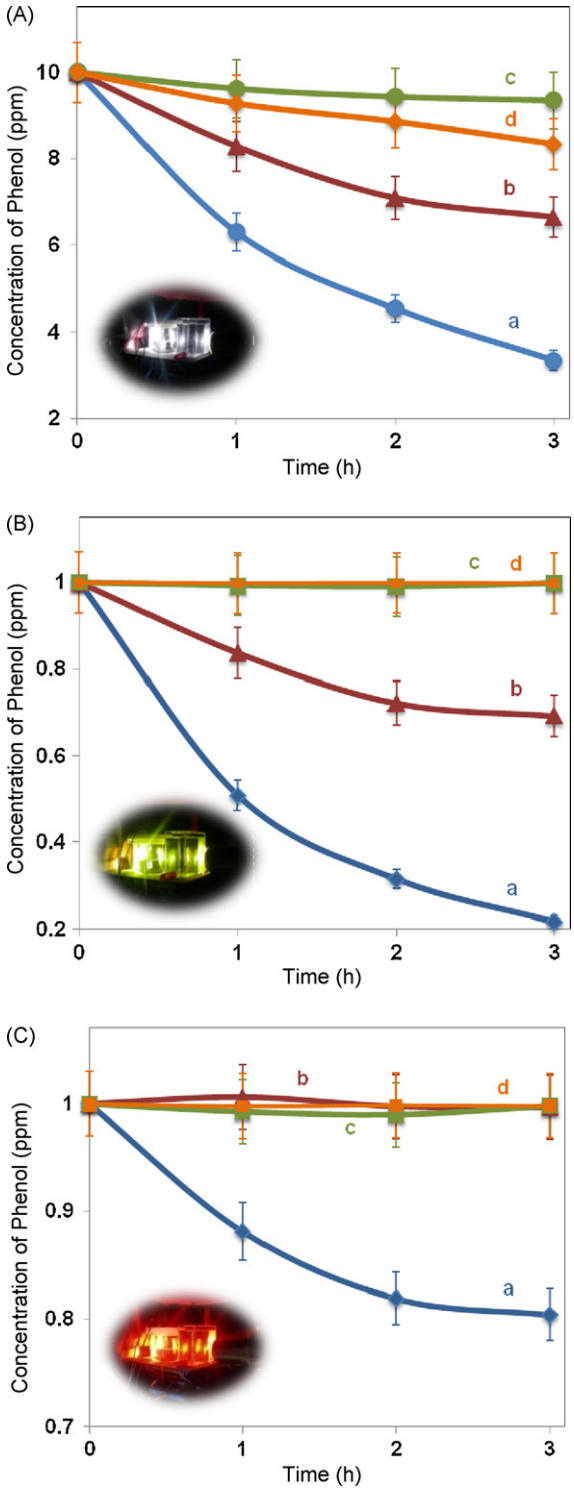

Fig. 7. Photo-catalytic decomposition of phenol under visible light irradiation. (A) White light (≥420 nm), (B) green light (≥500 nm), and (C) red light (≥600 nm); (a) C–TiO_2-250, (b) C–TiO_2-320, (c) C–TiO_2-450, and (d) commercial TiO_2 P25.

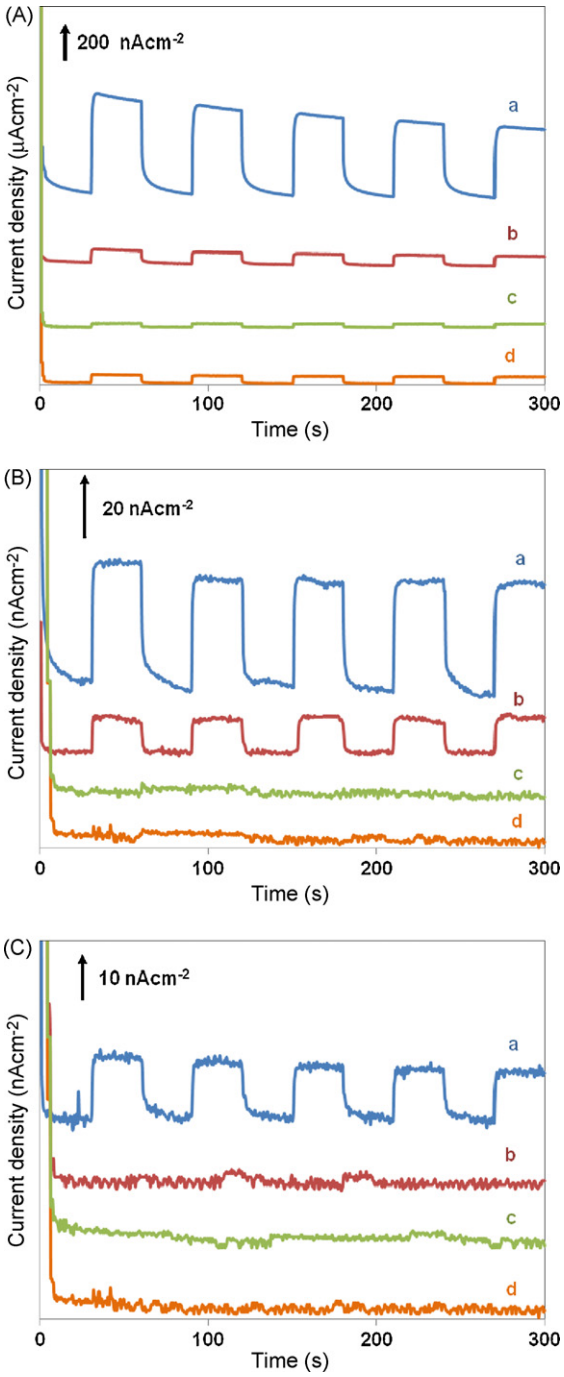

Fig. 8. Photo-generated current density of each sample under visible light irradiation. (A) White light (≥420 nm), (B) green light (≥500 nm), and (C) red light (≥600 nm); (a) C–TiO_2-250, (b) C–TiO_2-320, (c) C–TiO_2-450, and (d) commercial TiO_2 P25.

visible light irradiation, thus facilitating oxidation reactions [25,26]. The synergic effect of the lower E_g resulting from the carbon incorporated into the TiO_2 crystal lattice and photo-sensitizing resulting from the carbon adsorbed to C–TiO_2-250 leads a significant increase in photo-catalytic activities under visible light irradiation. In particular, 20% of 1 ppm phenol was decomposed by C–TiO_2-250 under red light irradiation with a long wavelength light (≥600 nm). C–TiO_2-450 did not show any decomposition under visible light since all of the incorporated carbons were removed after calcinations at 450 °C. These findings are in good agreement with current transient results performed with visible light turned on/off at 30 s intervals (Fig. 8). C–TiO_2-250 is capable of generating high photo-current densities (500 nA cm^{-2}) under visible light illumination (≥420 nm). They also generated a current density (15 nA cm^{-2}) under long wavelength light irradiation of ≥600 nm. The high current density for C–TiO_2-250 under visible light illumination results in a superior activity in the photo-catalytic decomposition of phenol. The photo-generated current density also decreases upon the subsequent elimination of photo-sensitizing carbon and doped carbon.

4. Conclusion

In summary, C–TiO_2 nanoparticles, for use as a visible light photo-catalyst, were readily synthesized using wet chemistry. The synergic effect of a lower band-gap energy and photo-sensitizing results in the C–TiO_2 nanoparticles that show highly efficient performances for photo-catalytic reactions under visible light. It can be a powerful advantage of C–TiO_2 when compared with N–TiO_2 because elemental nitrogen does not show photo-sensitizing effect. Especially, C–TiO_2 nanoparticles showed outstanding photo-catalytic activities under long wavelength-visible light irradiation even longer than 600 nm, thus such catalysts can be effectively used for both indoor and outdoor utilities. The findings reported herein, indicate the prospect of promising applications in environmental treatment and energy production, including photo-catalytic oxidization system, hydrogen evolution via water splitting, solar cells, etc. Further investigation to improve photo-catalytic performance and exploration for potential applications are in progress.

Acknowledgements

This research was supported by WCU (World Class University) program through the Korea science and Engineering Foundation funded by the Ministry of Education, Science and Technology (400-2008-0230). The authors especially appreciate to Dr. Mi-Young Kim (The Research Institute for Catalysis, Chonnam National University) for XANES and EXAFS measurement.

References

[1] A. Mills, R.H. Davies, D. Worsley, Chem. Soc. Rev. 22 (2003) 417–434.
[2] J. Perala, D.F. Ollisa, J. Catal. 136 (1992) 554–565.
[3] R.W. Matthews, S.R. McEvoy, Sol. Energy 49 (1992) 507–513.
[4] H.J. Yun, H. Lee, J.B. Joo, W. Kim, J. Yi, J. Phys. Chem. C 113 (2009) 3050–3055.
[5] A. Fujishima, K. Honda, Nature 238 (1972) 37–38.
[6] S. Sato, M. White, Chem. Phys. Lett. 72 (1980) 83–86.
[7] C.D. Jaeger, A.J. Bard, J. Phys. Chem. 83 (1979) 3146–3152.
[8] B. O'Regan, M. Grätzel, Nature 353 (1991) 737–740.
[9] S.H. Kang, S.-H. Choi, M.-S. Kang, J.-Y. Kim, H.-S. Kim, T. Hyeon, Y.-E. Sung, Adv. Mater. 20 (2008) 54–58.
[10] S. Ito, S.M. Zakeeruddin, P. Comte, P. Liska, D. Kuang, M. Grätzel, Nat. Photonics 2 (2008) 693–698.
[11] J. Joo, S.G. Kwon, T. Yu, M. Cho, J. Lee, J. Yoon, T. Hyeon, J. Phys. Chem. B 109 (2005) 15297–15302.
[12] X. Chen, S.S. Mao, Chem. Rev. 107 (2007) 2891–2959.
[13] R. Asahi, T. Morikawa, T. Ohwaki, K. Aoki, Y. Taga, Science 293 (2001) 269–271.
[14] W. Balcerski, S.Y. Ryu, M.R. Hoffmann, J. Phys. Chem. C 111 (2007) 15357–15362.
[15] D. Mitoraj, H. Kisch, Angew. Chem. Int. Ed. 47 (2008) 9975–9978.
[16] S. Kim, S.-J. Hwang, W. Choi, J. Phys. Chem. B 109 (2005) 24260–24267.
[17] J.A. Rengifo-Herrera, E. Mielczarski, J. Mielczarski, N.C. Castillo, J. Kiwi, C. Pulgarin, Appl. Catal. B: Environ. 84 (2008) 448–456.
[18] Z. He, X. Xu, S. Song, L. Xie, J. Tu, J. Chen, B.A. Yan, J. Phys. Chem. C 112 (2008) 16431–16437.
[19] S.U.M. Khan, M. Al-Shahry, W.B. Ingler Jr., Science 297 (2002) 2243–2245.
[20] D.-E. Gu, Y. Lu, B.-C. Yang, Y.-D. Hu, Chem. Commun. (2008) 2453–2455.
[21] G. Wu, T. Nishikawa, B. Ohtani, A. Chen, Chem. Mater. 19 (19) (2007) 4530–4537.
[22] J.H. Park, S. Kim, A.J. Bard, Nano Lett. 6 (2006) 24–28.
[23] I.-C. Kang, Q. Zhang, S. Yin, T. Sato, F. Saito, Appl. Catal. B: Environ. 80 (2008) 81–87.
[24] C. Di Valentin, G. Pacchioni, A. Selloni, Chem. Mater. 17 (2005) 6656–6665.
[25] X. Yang, C. Cao, L. Erickson, K. Hohn, R. Maghirang, K. Klabunde, J. Catal. 260 (2008) 128–133.
[26] C. Lettmann, K. Hildenbrand, H. Kisch, W. Macyk, W.F. Maier, Appl. Catal. B: Environ. 32 (2001) 215–227.
[27] T. Sugimoto, X. Zhou, A. Muramatsu, J. Colloid Interface Sci. 259 (2003) 43–52.
[28] T. Sugimoto, X. Zhou, A. Muramatsu, J. Colloid Interface Sci. 259 (2003) 53–61.
[29] F. Farges, G.E. Brown Jr., J.J. Rehr, Phys. Rev. B 56 (1997) 1809–1819.
[30] V. Schwartz, D.R. Mullins, W. Yan, H. Zhu, S. Dai, S.H. Overbury, J. Phys. Chem. C 111 (2007) 17322–17332.
[31] R. Kozlowski, R.F. Pettifer, J.M. Thomas, J. Phys. Chem. 87 (1983) 5172–5176.
[32] M.A. Butler, J. Appl. Phys. 48 (1977) 1914–1920.